Miniaturized fiber taper reflective interferometer for high temperature measurement

Jun-long Kou, Jing Feng, Liang Ye, Fei Xu,* and Yan-qing Lu

College of Engineering and Applied Sciences and National Laboratory of Solid State Microstructures, Nanjing University, Nanjing 210093, China
**feixu@nju.edu.cn*

Abstract: We present an ultra-small all-silica high temperature sensor based on a reflective Fabry-Perot modal interferometer (FPMI). Our FPMI is made of a micro-cavity (~4.4 μm) directly fabricated into a fiber taper probe less than 10 μm in diameter. Its sensing head is a miniaturized single mode-multimode fiber configuration without splicing. The sensing mechanism of FPMI is the interference among reflected fundamental mode and excited high-order modes at the end-faces. Its temperature sensitivity is ~20 pm/°C near the wavelength of 1550 nm. This kind of sensor can work in harsh environments with ultra-large temperature gradient, but takes up little space because of its unique geometry and small size.

OCIS codes: (060.2370) Fiber optics sensors; (120.6780) Temperature.

References and links

1. B. W. Zhang, and M. Kahrizi, "High-temperature resistance fiber Bragg grating temperature sensor fabrication," IEEE Sens. J. **7**(4), 586–591 (2007).
2. H. Y. Choi, K. S. Park, S. J. Park, U. C. Paek, B. H. Lee, and E. S. Choi, "Miniature fiber-optic high temperature sensor based on a hybrid structured Fabry-Perot interferometer," Opt. Lett. **33**(21), 2455–2457 (2008).
3. T. Wei, Y. K. Han, H. L. Tsai, and H. Xiao, "Miniaturized fiber inline Fabry-Perot interferometer fabricated with a femtosecond laser," Opt. Lett. **33**(6), 536–538 (2008).
4. Y. Z. Zhu, Z. Y. Huang, F. B. Shen, and A. B. Wang, "Sapphire-fiber-based white-light interferometric sensor for high-temperature measurements," Opt. Lett. **30**(7), 711–713 (2005).
5. A. Wang, S. Gollapudi, R. G. May, K. A. Murphy, and R. O. Claus, "Advances in sapphire-fiber-based intrinsic interferometric sensors," Opt. Lett. **17**(21), 1544–1546 (1992).
6. L. V. Nguyen, D. Hwang, S. Moon, D. S. Moon, and Y. Chung, "High temperature fiber sensor with high sensitivity based on core diameter mismatch," Opt. Express **16**(15), 11369–11375 (2008).
7. C. Zhan, J. H. Kim, J. Lee, S. Yin, P. Ruffin, and C. Luo, "High temperature sensing using higher-order-mode rejected sapphire-crystal fiber gratings," Proc. SPIE **6698**, 66980F (2007).
8. S. H. Nam, C. Zhun, and S. Yin, "Recent advances on fabricating in-fiber gratings in single crystal sapphire fiber," Proc. SPIE **5560**, 147–155 (2004).
9. J. Wang, B. Dong, E. Lally, J. Gong, M. Han, and A. Wang, "Multiplexed high temperature sensing with sapphire fiber air gap-based extrinsic Fabry-Perot interferometers," Opt. Lett. **35**(5), 619–621 (2010).
10. D. Monzon-Hernandez, V. P. Minkovich, and J. Villatoro, "High-temperature sensing with tapers made of microstructured optical fiber," IEEE Photon. Technol. Lett. **18**(3), 511–513 (2006).
11. H. Y. Choi, K. S. Park, S. J. Park, U.-C. Paek, B. H. Lee, and E. S. Choi, "Miniature fiber-optic high temperature sensor based on a hybrid structured Fabry-Perot interferometer," Opt. Lett. **33**(21), 2455–2457 (2008).
12. H. Y. Choi, G. Mudhana, K. S. Park, U. C. Paek, and B. H. Lee, "Cross-talk free and ultra-compact fiber optic sensor for simultaneous measurement of temperature and refractive index," Opt. Express **18**(1), 141–149 (2010).
13. J. Villatoro, V. Finazzi, G. Coviello, and V. Pruneri, "Photonic-crystal-fiber-enabled micro-Fabry-Perot interferometer," Opt. Lett. **34**(16), 2441–2443 (2009).
14. T. Wei, Y. Han, Y. Li, H.-L. Tsai, and H. Xiao, "Temperature-insensitive miniaturized fiber inline Fabry-Perot interferometer for highly sensitive refractive index measurement," Opt. Express **16**(8), 5764–5769 (2008).
15. Y.-J. Rao, M. Deng, D.-W. Duan, X.-C. Yang, T. Zhu, and G.-H. Cheng, "Micro Fabry-Perot interferometers in silica fibers machined by femtosecond laser," Opt. Express **15**(21), 14123–14128 (2007).
16. F. Renna, D. Cox, and G. Brambilla, "Efficient sub-wavelength light confinement using surface plasmon polaritons in tapered fibers," Opt. Express **17**(9), 7658–7663 (2009).
17. J. D. Love, W. M. Henry, W. J. Stewart, R. J. Black, S. Lacroix, and F. Gonthier, "Tapered single-mode fibres and devices. Part 1: Adiabaticity criteria," IEE Proc., J Optoelectron. **138**(5), 343–354 (1991).

#128567 - $15.00 USD Received 17 May 2010; revised 15 Jun 2010; accepted 15 Jun 2010; published 17 Jun 2010

1. Introduction

Optical fiber temperature sensors have been studied extensively over the last two decades due to its light weight, flexibility, good electromagnetic interference immunity and low cost [1–5]. A considerable number of such sensors have been developed based on different technologies, such as fiber-grating-based and interferometer-based systems with standard silica fiber [6], sapphire fiber [7–9], and photonic crystal fiber [10,11]. Among them, the air-gap micro-cavity based Fabry-Perot interferometer (AG-MC-FPI) sensors are particularly attractive for high temperature sensing owing to their low cost, simple configuration, small cross sensitivity, miniature sensor head, flexibility in the tuning of sensitivity, and dynamic range. The air-gap can be assembled by inserting two sapphire fiber into a zirconia tubes [9], splicing a single mode fiber (SMF) and a multimode fiber (MMF) or photonic crystal fiber (PCF) to a hollow-core fiber [2,12], or splicing an SMF and an index-guiding PCF together [13]. Complicated fabrication process, expensive special fibers, poor reproducibility, possible mismatch between different parts and difficulty in precise control of the cavity length are disadvantages of these interferometer fabricating techniques. What's more, in some systems, complex and expensive fringe counting techniques must be employed for mathematical post-processing of the acquired data. And the lengths of these micro-air-gap cavities are limited to above tens of micrometers and the lengths of sensing areas are in the order of millimeter accordingly.

Recently femtosecond laser fabrication method has attracted much interest in micromachining area especially for smaller air-gap micro-cavity devices. Many researchers have reported micromachining notch-like micro-cavities in SMFs to form FPIs for sensing in this way [14,15]. However, these sensors exhibited low temperature sensitivity (~1 pm/°C) possibly because of single mode operation in the thick SMF, and small fringe visibility caused by the rugged surfaces of the micro-cavity [14,15]. Moreover the cavity lengths are still in the order of tens of micrometers.

In this paper, we present an alternative to fabricate ultra-small AG-MC-FPIs for high-temperature sensing by focused ion beam (FIB) machining in SMF taper tips (SMF-TTs). FIB technology is perfect for micro-machining and nano-fabrication due to its small and controllable spot size (55 nm in our milling process) and high beam current density. It is possible to directly micromachine a micro-cavity directly in a subwavelength fiber by FIB [16]. An SMF-TT consists of an SMF and an MMF in nature, without splicing. And it is possible to use an SMF-TT as a highly sensitive modal interferometer. Here we directly machine a micro-notch cavity on an SMF-TT, where it is around 9 μm in diameter. This cavity is within several micrometers in length, height and width. The light at the end-faces of the cavity is reflected and possibly excited into high-order modes due to modal mismatch. The all-glass FP modal interferometer (FPMI) has a temperature sensitivity of about 20 pm/°C. Its extremely small size, all fiber connection, high sensitivity and especially unique structure offer great potentials for fast-response high temperature sensing particularly in small and harsh area with high temperature gradient. However its ability to work in harsh environment is probably limited because it is brittle and easy to get dirty. Suitable packaging technique still should be further developed for a practical device to keep the sensing head clean and prevent broken.

2. Fabrication of the SMF-TT FPMIs

The fabrication of the SMF-TT is carried out with a commercial pipette puller (model P2000) [16]. CO_2 laser power and pulling velocity are optimized to achieve an optimum taper profile. The manufactured SMF-TT has a long pigtail to allow prompt link to other optical fiber component. The tip is first coated with a 150 nm-thick layer of aluminum (Al) through vacuum evaporation deposition . The Al layer is used as a conductive layer to prevent gallium ion accumulation in the FIB micromachining process. Figure 1 shows a photograph of the SMF-TT in our experiment, by combining five photographs at different positions, because the taper

#128567 - $15.00 USD Received 17 May 2010; revised 15 Jun 2010; accepted 15 Jun 2010; published 17 Jun 2010

length is much longer than the fiber diameter. The total length of the taper transition is about 2.1 mm and the tip diameter is less than 1 μm.

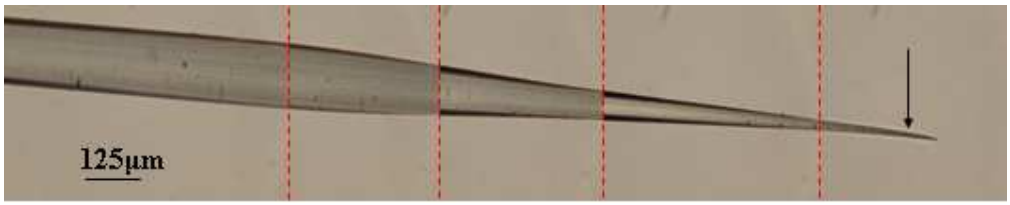

Fig. 1. Microscope image of the SMF-TT in our experiment, five photographs separated by four dashed vertical lines are used to show the whole profile of the SMF-TT. The black arrow indicates the location of the micro-notch.

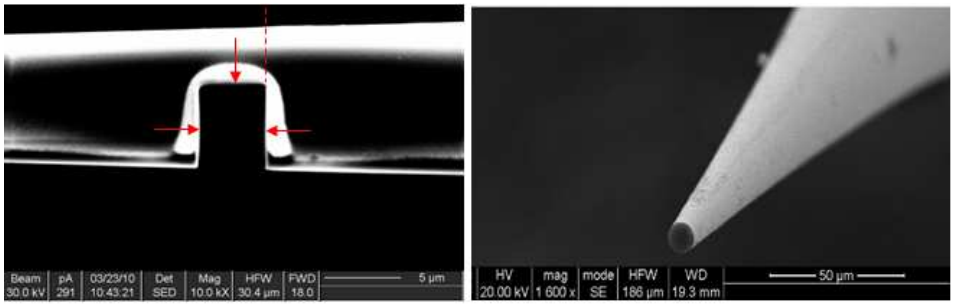

Fig. 2. SEM image (a) of the micro-notch cavity from the side view: three arrows show the edges of the cavity at the fiber tip, (b) of the cross section with the fiber tip cleaved at the position indicated in (a) by a dash line.

Then, the Al-coated fiber tip is placed steadily in the FIB machining chamber (Strata FIB 201) using a conductive tape. We use a 30.0 kV, 291 pA gallium ion beam perpendicular to the fiber axis. The shape of the beam is cylindrical symmetric with a diameter of about 55 nm. With such accuracy, cavity length can be controlled precisely. It also enables us to fabricate a micro-notch with sharp end-faces of the cavity. In our experiment, the cavity is made from a two-step process. Because there are some remains adhering onto the surfaces of the cavity after the first milling step, a second step under the same beam current is used to improve the surface smoothness. Figure 2 shows an SEM picture of the micro-notch cavity from the side view and cross section after cleaving the SMF-TT at the cavity. The end-face is very sharp and smooth. The cavity is 4.4 μm long and 5 μm high, located at the position with the local radius $r = 4.6$ μm. Finally, the fiber tip is immersed in hydrochloric acid for about 30 minutes to totally remove the Al layer before it is cleaned with deionized water.

3. Experiment and discussion

The reflective spectral response of this FPMI device in Fig. 1 and 2 is measured with a broadband source (1525 ~1610 nm) and an Ando AQ6317B optical spectrum analyzer (OSA) through a circulator. The SMF-TT without a cavity displays an ignorable reflection of less than −100 dB over the whole broadband spectrum. Hence, the detected signal is the light reflected only at the two end-faces of the micro-cavity, and the reflection at the tip end is negligible. We characterize the thermal response of the FTMI device by heating it up in a micro-furnace (FIBHEAT200, Micropyretics Heaters International Inc.) and the temperature ranging from room temperature (19 °C) to 520 °C is measured by a thermocouple (TES-1310, Type K, TES Electrical Electronic Corp.). The spectrum and temperature were recorded when both of them are stable for several minutes.

The interference spectra of the FPMI device at different temperatures (19 °C, 305 °C and 520 °C) are shown in Fig. 3. The spectra indicates a free spectral range (FSR) of ~11 nm and a

#128567 - $15.00 USD Received 17 May 2010; revised 15 Jun 2010; accepted 15 Jun 2010; published 17 Jun 2010

fringe visibility of ~11 dB around 1550 nm, which is larger than some other high-temperature AG-MC-FPI sensors [2,9], and enough for sensing application.

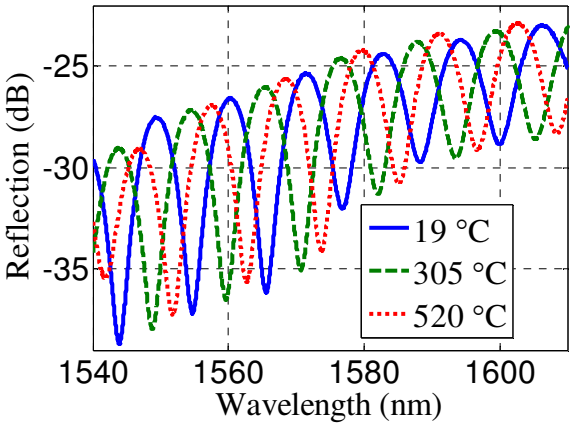

Fig. 3. Interference spectra of the FPMI device in air at different temperatures.

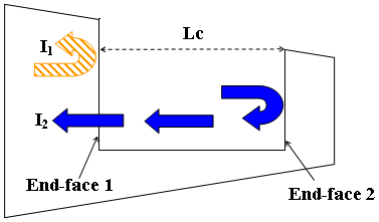

Fig. 4. Illustration of the FPMI. I_1 and I_2 are the reflections at end-face 1 and end-face 2 respectively; L_c is the length of the cavity. When I_2 enters end-face 1, the fundamental mode is possible to be excited to a higher-order mode.

Due to the low reflectivity of the air-glass interfaces, multiple reflections have negligible contributions to the optical interference. As shown in Fig. 4, we only consider two reflections I_1 and I_2 at the two end-faces, respectively. However, a fiber taper may hold both the original single core mode and the multi-modes in the cladding at different positions. The fundamental LP_{01} mode can be coupled to high-order LP_{0m} mode in the taper transition or be excited to high-order LP_{0m} mode at the end-faces. I_1 or I_2 possibly include LP_{01} or LP_{0m} mode. We also break the cavity and measure the reflection I_1 at end-face 1; flat reflective spectrum without obvious interference fringes is observed. Accordingly, a reasonable assuming is to consider only one dominated mode in I_1 (LP_{01} mode) and I_2 (LP_{01} or LP_{0m} mode excited when inputting I_2 into end-face 1). The interference spectrum can be modeled using the following two-beam optical interference equation:

$$I = I_1 + I_2 + 2\sqrt{I_1 I_2}\cos(\delta + \varphi_0). \tag{1}$$

The phase difference between two modes in I_1 and I_2 is

$$\begin{cases} \delta = \delta_1 + q\delta_2 = (2\pi/\lambda)(\Delta_1 + q\Delta_2), \\ \Delta_1 = 2n_c L_c, \\ \Delta_2 = \int (n_2(r) - n_1(r))dz(r), \end{cases} \tag{2}$$

and FSR is

#128567 - $15.00 USD Received 17 May 2010; revised 15 Jun 2010; accepted 15 Jun 2010; published 17 Jun 2010

$$FSR = 2\pi\lambda / \delta, \tag{3}$$

where $q = 0$ (for LP_{01} in I_2) and 1 for (LP_{0m} in I_2); Δ_1 (δ_1) and Δ_2 (δ_2) are the optical path length difference (the phase difference) owing to the micro-cavity and the modal difference in the taper transition, respectively; $n_1(r)$ and $n_2(r)$ are the effective index of LP_{01} and LP_{0m} modes, respectively, functions of local radius $r(z)$ of the microfiber probe at position z, which can be calculated by three-layer model of finite cladding step-profile fiber with the microfiber probe profile $r(z)$ which can be obtained from Fig. 1 [17]. δ_1 is ~12 π and δ_2 ~295 π for LP_{03} mode, and FSR ~10 nm, in good agreement with what we obtain in the experiment. In our calculation, λ = 1530 nm, L_c = 4.4 μm and n_c = 1.

The temperature sensitivity S is defined as the interference wavelength shift divided by the corresponding temperature change. S depends on temperature through the thermal expansion and/or thermo-optics effect [2]:

$$\begin{cases} S = \dfrac{d\lambda}{dT} = \dfrac{2\pi}{\delta}\left(\dfrac{d\Delta_1}{dT} + \dfrac{d\Delta_2}{dT}\right) = \dfrac{2\pi}{\delta}\left(2\alpha_T L_c + \dfrac{d\Delta_2}{dT}\right), \\ \dfrac{d\Delta_2}{dT} \simeq \int \left[\dfrac{\partial(n_1 - n_2)}{\partial n}\sigma_T + \dfrac{\partial(n_1 - n_2)}{\partial r}\alpha_T\right]dz, \end{cases} \tag{4}$$

where σ_T (1.1×10^{-5} /°C) is the thermo-optics coefficient and α_T (5.5×10^{-7} /°C) is the thermal expansion coefficient. There are two contributions from temperature change: the temperature-induced length variation in the cavity, and the temperature-induced index variation and taper volume variation in taper transition. The first one is less than 1 pm/°C and ignorable, it agrees with the fact that those previous micro-cavity FP interferences in SMF by femtosecond laser machining are temperature-insensitive; the second one is about 10 ~20 pm/°C and dominates in temperature sensing.

Figure 5 displays the measured interferometer wavelength shifts (Δλ) and error on temperature (T). As the temperature increases, the interferometer wavelength shifts to longer wavelength. A third-order polynomial was used to fit the wavelength shifts across the entire calibration range. The average sensitivity of the device is ~17 pm/°C, which is very close to the theoretical result. The solution could be estimated to be ~0.58°C with the OSA resolution of 0.01 nm. Higher sensitivity can be obtained by optimizing the profile of the SMF-TT or use special fiber taper with higher thermo-optics coefficient. The error is smaller than 5% when the temperature is above 100 °C.

#128567 - $15.00 USD Received 17 May 2010; revised 15 Jun 2010; accepted 15 Jun 2010; published 17 Jun 2010

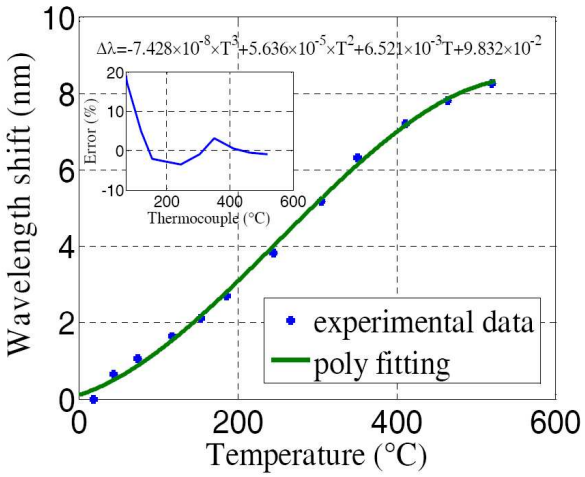

Fig. 5. Dependence of the measured wavelength shift on temperature. The asterisk represents the measured results while the solid line is the fitting result. The inset shows the dependence of error on temperature.

4. Conclusion and discussion

We have demonstrated an ultra-small all-silica SMF-TT interferometer, with an open 4 μm-micro-cavity fabricated by focused ion beam (FIB) micromachining, for fast-response high temperature sensing. It is one kind of modal FP interferometer resulting from the interference among the reflected fundamental mode and excited high-order modes. Its extinction ratio is above 10 dB, FSR is about 11 nm, and sensitivity is nearly 20 pm/°C. Its advantages of compact size, high sensitivity, easy interrogation, simple fabrication and unique geometry, offer great prospects of developing practical high temperature sensors for ultra-small space and large temperature gradient in harsh environments, such as micro-flame and high temperature gas-phase/liquid-phase flow in microfluidics channel. Taking the benefit of so small thermal mass, it could react instantly to rapid thermal changes. In our experiments, an OSA is used to detect the wavelength shift, but it is relatively slow. To fully take the advantage of our sensor's potentials, a detector array based spectrum analyzer could be used. In these kinds of spectrometers, the signal is diffracted with a fixed grating then focused onto an InGaAs arrayed detector with multi-pixels. Because there is no moving parts like in an OSA, frequency response up to KHz could be achieved, which is desired to integrate with our sensor technology for fast response thermal measurement. Of course, there are still some possible disadvantages of our sensor: the tip is fragile especially after a notch is formed. The sensor may be broken due to simple handling or to vibrations that are often encountered in real industrial applications. Our future work is to encapsulate the sensor head to protect it and prevent dust particles or fluids condense into the cavity, thus improving its working stability.

Acknowledgment

This work is sponsored by the National 973 Program under contracts 2010CB327800 and 2006CB921805 and by the National Science Foundation of China (NSFC) under contracts 60977039 and 10874080. The authors also acknowledge the support by the Program for New Century Excellent Talents in University and the Changjiang Scholars Program. We also thank Qian-Jin Wang's technical support.

#128567 - $15.00 USD Received 17 May 2010; revised 15 Jun 2010; accepted 15 Jun 2010; published 17 Jun 2010